高等学校化学学报
CHEMICAL JOURNAL OF CHINESE UNIVERSITIES
研究论文

# 超声调控的细胞膜表面氧化还原反应促进纳米粒摄取和内涵体逃逸

李　瑶[1#]，翟婉莹[1#]，王　征[1]，Petrov Alexey M.[2]，张葆鑫[3]，赵燕军[1]
（1. 天津大学药物科学与技术学院，天津市现代药物传递及功能高效化重点实验室，天津 300072；
2. 俄罗斯喀山国立医科大学，喀山 420012；3. 内蒙古医科大学第二附属医院，呼和浩特 010000）

**摘要**　细胞摄取和内涵体逃逸是纳米药物递送的两个关键屏障. 研究发现，细胞外表面的硫醇可以通过巯基-二硫化物/二硒化物交换反应同时克服这两个屏障. 然而，该策略增强纳米药物递送的能力有限. 为了解决上述问题，本文采用机械力(超声)来提高硫醇-二硫化物/二硒化物交换反应的动力学，进而提高药物递送效率. 研究结果为提高纳米药物递送效率提供了新方法.

**关键词**　氧化还原反应；细胞摄取；内涵体逃逸；纳米药物
**中图分类号**　O69；R943　　**文献标志码**　A　　doi：10.7503/cjcu20240265

# Ultrasound-aided Cellular Uptake and Endosomal Escape of Nanoparticles *via* the Membrane Surface Redox Reaction

LI Yao[1#], ZHAI Wanying[1#], WANG Zheng[1], Petrov Alexey M.[2],
ZHANG Baoxin[3*], ZHAO Yanjun[1*]
(*1. Tianjin Key Laboratory for Modern Drug Delivery & High Efficiency, School of Pharmaceutical Science & Technology, Tianjin University, Tianjin* 300072, *China*;
*2. Kazan State Medial University, Kazan RT* 420012, *Russia*;
*3. the Second Affiliated Hospital of Inner Mongolia Medical University, Hohhot* 010000, *China*)

**Abstract**　Cellular uptake and endosomal escape are two critical biological barriers to nanoscale drug delivery. The exofacial thiols at cell surface have been previously reported to simultaneously overcome these two barriers *via* the thiol-disulfide/diselenide exchange reaction. However, the power of such approach for nanomedicine delivery enhancement was limited. To address the above issue, we employed the mechanical force (ultrasound) that could significantly enhance the kinetics of thiol-disulfide/diselenide exchange reactions, and then the delivery efficiency. The discovery in the current work opens new avenues of tailored nanomedicine design to circumvent the delivery hurdles.

**Keywords**　Redox reaction; Cellular uptake; Endosomal escape; Nanomedicine

收稿日期：2024-05-31. 网络首发日期：2024-07-01.

联系人简介：赵燕军，男，博士，教授，主要从事应答响应型药物递送系统和基于铁死亡机理的疾病防治方面的研究.
E-mail: zhaoyj@tju.edu.cn
张葆鑫，男，博士，副主任医师，主要从事骨缺损和骨质疏松治疗方面的研究. E-mail: 197218725@qq.com

基金项目：国家自然科学基金(批准号：22075198，22175130)、内蒙古科技厅科技计划项目(批准号：2021GG0174，2020GG0195)和支持地方高校改革发展资金(学科建设)资助.
Supported by the National Natural Science Foundation of China(Nos. 22075198, 22175130), the Inner Mongolia Commission of Science and Technology Department, China(Nos. 2021GG0174, 2020GG0195), and the Fund for the Reforming and Development of Local Colleges and Universities(Discipline Construction), China.

# 共同第一作者.

# 1 Introduction

The rapid advance of nanotechnology has revolutionized the biomedical and pharmaceutical fields[1]. The nanoparticulate drug delivery usually faces sequential biological barriers, including mononuclear phagocyte system, non-specific biodistribution, hemorheological limitation, interstitial fluid pressure, cellular uptake, endosomal escape and multidrug resistance[2]. Among these, the extent to which nanocarrier internalization and escape from endosomes/lysosomes is essential for the therapeutic efficacy. The employment of targeting ligands is the well-known approach for the enhancement of cellular uptake *via* receptor-mediated endocytosis[3]. A variety of mechanisms of nanocarrier endosomal escape has been proposed, such as the proton sponge effect[4]. However, the enhancement methods of internalization and endosome escape is often dissected, which necessitates a complex nanocarrier design, leading to the difficulty of product quality control and scale-up manufacture.

The redox-active proteins(*e. g.* protein disulfide isomerases) on the cell surface, particularly cancer cell surface, offers the thiols groups towards the extracellular matrix for the alteration of protein function and activation of signaling pathways[5]. Such function is usually realized by the thiol-disulfide exchange reaction at the plasma membrane, which has been employed for the enhanced uptake of imaging agents, active therapeutics, proteins, nanobodies, liposomes, polymersomes and various types of nanocarriers[6—11]. The thiol-mediated cargo uptake can be manipulated by the strained disulfides[12—14]. Meanwhile, the thiol-disulfide exchange has been proved as a route for endosomal escape of polymeric nanocarriers. The covalent contact between the membrane thiols and the nanocarriers strains the packing of the endosomal membranes, and the propensity to relieve this strain is presumably the driving force for endosomal escape[15]. Nevertheless, the reaction kinetics of thiol-disulfide exchange is very slow (in the order of $k$=0.1—10 L·mol$^{-1}$·s$^{-1}$ at pH of 7), limiting the efficiency of nanocarrier uptake and escape from endosomes[16—18]. To address this, diselenolane-mediated cellular uptake was employed due to the improved reaction kinetics between thiols and diselenide[19,20].

It is generally believed that the mechanism of thiol-disulfide exchange reaction involves the $S_N2$ type nucleophilic substitution *via* a linear —S—S—S— like transition state[17]. Despite the fact that the thiol-disulfide exchange reaction is thermodynamically favorable, the activation energy should be overcome to form the transition state complex[21]. The polysulfide bonds are inherently sensitive to mechanical force[22]. Therefore, it was hypothesized that ultrasound may be employed to modulate the kinetics of thiol-disulfide/diselenide exchange reactions, and enhance the cellular uptake and endosomal escape of nanomedicines.

# 2 Experimental

## 2.1 Materials and Measurements

α-Tocopherol polyethylene glycol succinate (TPGS), Tokyo Chemical Industry Co., Ltd.; suberic acid (99%), 3,3′-dithiodipropionic acid (99%), 4-dimethylaminopyridine (DMAP, 99%), 5,5′-dithiobis(2-nitrobenzoic acid) (DTNB, 98%), iodoacetate (98%), Heowns Biochemical Technology Co., Ltd.; 3,3′-diselenodipropanoic acid (93%), Famris Pharmaceutical Technology Co., Ltd.; dicyclohexylcarbodiimide (DCC, 99%), Aladdin Bio-Chem Technology Co., Ltd.; fluorescein isothiocyanate (FITC, 90%), Sigma-Aldrich Chemical Reagent Co., Ltd.; Dulbecco's modified Eagle's medium (DMEM), fetal bovine serum, penicillin-streptomycin liquid (100×, cell culture grade), pancreatin (0.25%), cell counting kit-8 (CCK-8), dimethyl sulfoxide (DMSO, cell culture grade), Baibei Biotechnology Co., Ltd.; 5-(*N*-ethyl-*N*-isopropyl) amiloride (EIPA, 99%), chlorpromazine (CPZ, 10 mmol/L in DMSO), methyl-β-cyclodextrin (MβCD, 98%), Shanghai Macklin Biochemical Co., Ltd.; LysoTracker® Deep Red (1 mmol/L in DMSO), Yeasen

Institution of Biotechnology Co., Ltd. All standard solvents were sourced from Concord Tech Co., Ltd. All other chemicals were sourced from Guangfu Fine Chemical Research Institute.

Electronic analytical balance (AL204), Mettler-Toledo International Inc.; Nuclear magnetic resonance spectrometer (AVANCE III, NMR), Bruker Corporation; heating magnetic stirrer (C-MAG HS 7), IKA Ltd.; fluorescence spectrometer (Fluorolog 3-21), HORIBA Jobin Yvon Ltd.; high-performance liquid chromatography (HPLC, Waters e2695), Waters Technology Ltd.; Vacuum Freeze-Drying Dryer (FD-1), Beijing Biocool Experimental Instrument Co., Ltd.; Nano-ZS nanometer size and zeta analyzer (ZS 90), Malvern Instrument Ltd.; ultrasonic cell disruptor (JY88-II), Ningbo Xinzhi Biotechnology Co., Ltd.; desktop high speed centrifuge (H1850), Hunan Xiangyi Laboratory Instrument Development Co., Ltd.; $CO_2$ Incubator (HERAcell 240i), Thermo Fisher Scientific Inc.; biosafety cabinet (Opti·MAIRTM), Esco Ltd.; confocal laser scanning microscope (CLSM, TCS SP8), Leica Microsystems Inc., IL.

### 2.2 Methods

2.2.1 Synthesis of TPGS Conjugates 174.8 mg (0.12 mmol) TPGS, 20.35 mg (0.12 mmol) suberic acid or 24.56 mg (0.12 mmol) 3,3′-dithiodipropionic acid or 35.51 mg (0.12 mmol) 3,3′-diselenodipropanoic acid and 5.71 mg (0.05 mmol) DMAP were added into 10 mL mixed solvent of anhydrous dichloromethane (DCM) and *N*,*N*-dimethylformamide (DMF) (volume ratio, 1∶1) and stirred magnetically for 30 min. Then 26.51 mg (0.13 mmol) DCC was induced for further 1 h in the ice bath followed by shifting the system to ambient temperature to stir for 24 h more, the reaction was monitored by thin layer chromatography (TLC) ($V_{Methanol}$∶$V_{DCM}$=2∶8). Upon completion, the mixture was filtered and washed by two cycles of water (100 mL) and one cycle of brine (100 mL), dried using anhydrous $Na_2SO_4$ before evaporation and finally recrystallized in diethyl ether.

2.2.2 Manufacture and Characterization of Micelles The micelles were fabricated through the membrane-hydration method. Briefly, 14.27 μmol FITC was dispersed into 20 mL methanol containing 50 mg dissolved modified TPGS in sequence, followed by vertexing. The solid film was hydrated by 20 mL deionized water after removing solvent by rotary evaporation. Then the excess FITC was removed by centrifugation (3823*g*, 10 min) and filtration through a 0.45 μm membrane prior to lyophilization [FITC-control micelles (CM), FITC-disulfide-bearing micelles (SM), FITC-diselenide-bearing micelles (SeM), respectively]. The placebo micelles were fabricated without the supplement of FITC (CM, SM, SeM, respectively). Then the blank micelles and FITC-loaded micelles (both at 0.5 mg/mL) were characterized in terms of dynamic light scattering and zeta potential (ζ). The amount of FITC in micelles was determined by high performance liquid chromatography.

2.2.3 Cell Culture The human cervical cancer cells (Hela) were provided by the State Key Laboratory of Medicinal Chemical Biology (Nankai University). Hela cells were cultured in DMEM medium containing fetal bovine serum in a volume fraction of 10% and penicillin/streptomycin in a volume fraction of 1%. The cell lines were incubated in an incubator at 37 ℃ containing 5% (volume fraction) $CO_2$.

2.2.4 Investigation of Endocytosis Pathway To clarify the endocytosis pathway of these micelles with different decorative structures, various endocytosis inhibitors were introduced. First, the cytotoxicity of various inhibitors was investigated by CCK-8 assay. Briefly, Hela cells were seeded in 96-well plates at a density of $4\times10^3$ per well for 24 h, followed by the incubation with different formulations including EIPA (20 μmol/L), CPZ (10 μg/mL), MβCD (2 mmol/L), DTNB (1 mmol/L) and iodoacetate (1 mmol/L) for 1.5 h prior to colorimetric CCK-8 assay. Subsequently, the influence of various inhibitors on cellular uptake of FITC-loaded micelles (FITC-CM, FITC-SM and FITC-SeM) were investigated. In brief, Hela cells were cultured in 6-well plates at a density of $5\times10^5$ per well for 24 h, then the cells were incubated with different

inhibitors for 0.5 h, followed by the incubation of FITC-CM, FITC-SM or FITC-SeM (at FITC concentration of 20 μmol/L) in the presence of inhibitors for another 1 h. To investigate the influence of temperature on cellular uptake, cells were incubated with FITC-CM, FITC-SM or FITC-SeM at 4 ℃ for 1 h. Finally, cells were washed with cold phosphate buffer saline (PBS) and centrifuged (156*g*, 3 min), followed by sonication at 4 ℃ for 10 min. The FITC quantification was measured through high performance liquid chromatography. The total protein was determined *via* Bradford protein assay kit following the manufacturer's instructions. The FITC quantification was finally normalized to total protein. All experiments were carried out in triplicate, and cells without the presence of inhibitors were used as control.

2.2.5 Effect of Conjugate Structures and Ultrasound on Cellular Uptake Hela cells were seeded in 6-well plates at a density $5\times10^5$ per well for 24 h, followed by a new culture medium contained different formulations including FITC-CM, FITC-SM and FITC-SeM micelles (at FITC concentration of 20 μmol/L) respectively supplemented. After 0.5 h, the application of ultrasonic action was performed (1 MHz, 1.0 W/cm$^2$, 20% duty cycle, 120 s) and the cells were further incubated for 2 h. Finally, cells were washed with cold PBS and then collected, the subsequent quantitative analysis was consistent with the previous experiment. All experiments were carried out in triplicate.

2.2.6 Effect of Conjugate Structures and Ultrasound on Endosomal Escape Hela cells were seeded in 20 mm plates at a density of $8\times10^4$ per well, for 24 h and then incubated with FITC-CM, FITC-SM and FITC-SeM micelles (at FITC concentration of 5 μmol/L) respectively. After 0.5 h, the application of ultrasonic action was performed (1 MHz, 1.0 W/cm$^2$, 20% duty cycle, 120 s). After 2 h, the extracellular nanocarriers were washed and LysoTracker® Deep Red (50 nmol/L) in serum-free medium was added to stain lysosomes for 30 min, the unbound dyes were removed and rinsed by PBS in triplicate and then imaged by a Leica TCS SP8 confocal laser scanning microscope (FITC: $\lambda_{ex}/\lambda_{em}$ 488/500—530 nm, LysoTracker® Deep Red: $\lambda_{ex}/\lambda_{em}$ 552/580—600 nm). Image processing and colocalization analyses were performed using the Image J software. Colocalization was expressed as the Pearson's correlation coefficient (R). All experiments were carried out in triplicate.

2.2.7 Statistical Analysis All data were presented as the mean±standard deviation (SD). The difference was statistically compared *via* the Student's t test or analysis of variance integrated with the Tukey's post-hoc analysis. The critical $p$ value was set at 0.05.

## 3 Results and Discussion

### 3.1 Preparation of Nano-Micelles

To prove the above hypothesis, we prepared three types of micellar nanocarriers (Scheme 1). The micelles were produced by self-assembly of the derivatives of *D*-α-tocopheryl polyethylene glycol succinate (TPGS). The TPGS was chemically modified by octanedioic acid, 3,3′-disulfanediyldipropionic acid, and 3,3′-diselanediyldipropionic acid, respectively (Scheme S1, see the Supporting Information of this paper).

The successful synthesis of three TPGS derivatives was confirmed by the proton and carbon nuclear magnetic resonance spectroscopy ($^1$H NMR and $^{13}$C NMR) (Figs.S1—S8, see the Supporting Information of this paper). These amphiphilic TPGS derivatives were the building block of CM, SM, and SeM [Fig.1(A)]. A fluorescent probe, fluorescein (FITC) was physically encapsulated in these micelles, producing FITC-CM, FITC-SM, and FITC-SeM, respectively. Dynamic light scattering showed that there was no significant difference among the hydrodynamic size of all blank micelles (*ca.* 15 nm); upon FITC loading, the size of micelles equivalently increased to *ca.* 22 nm [Fig.1(B)]. This was because the cargo-induced expansion of micellar core. All six types of micelles are slightly negatively charged, as verified by the zeta potential analysis

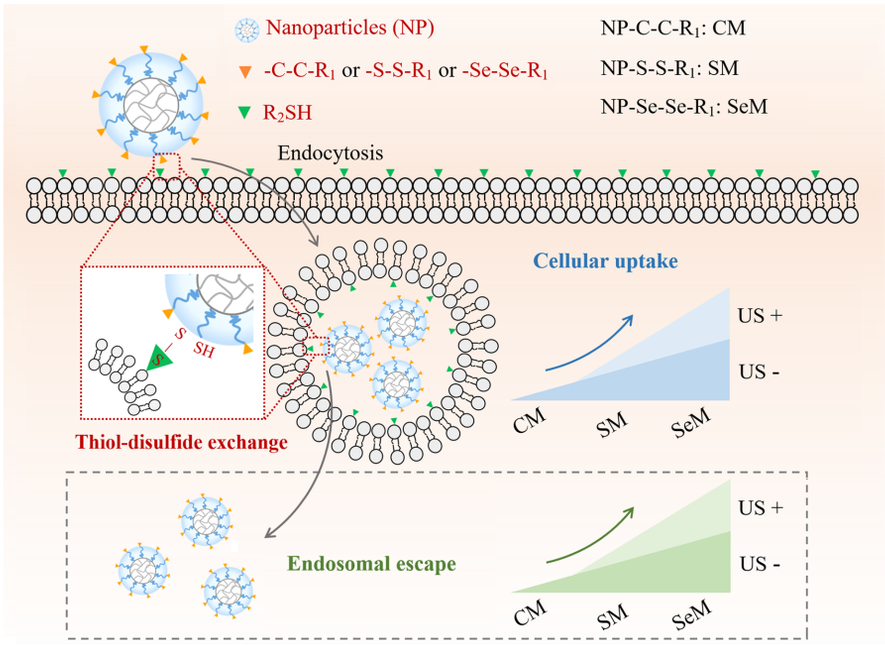


**Scheme 1 Schematic illustration of ultrasound-aided simultaneous cellular uptake and endosomal escape of nanoparticles that are surface-engineered with either disulfide or diselenide moieties**

The corresponding mechanism is the enhancement of membrane surface redox reaction kinetics between thiol and disulfide/diselenide. CM: control micelles; SM: disulfide-bearing micelles; SeM: diselenide-bearing micelles; US: ultrasound.

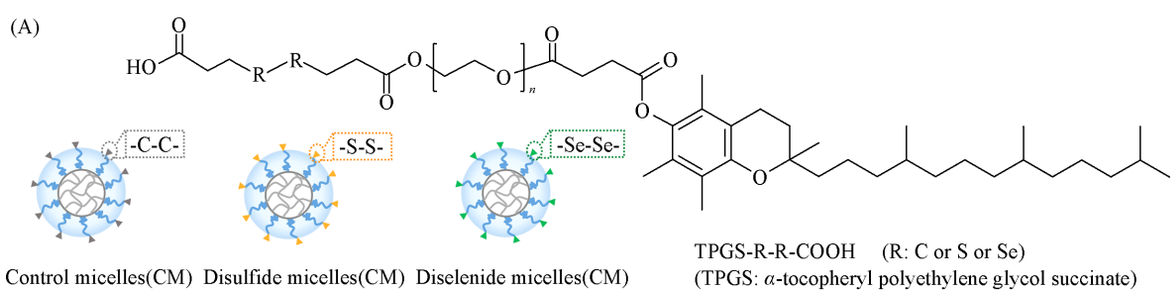


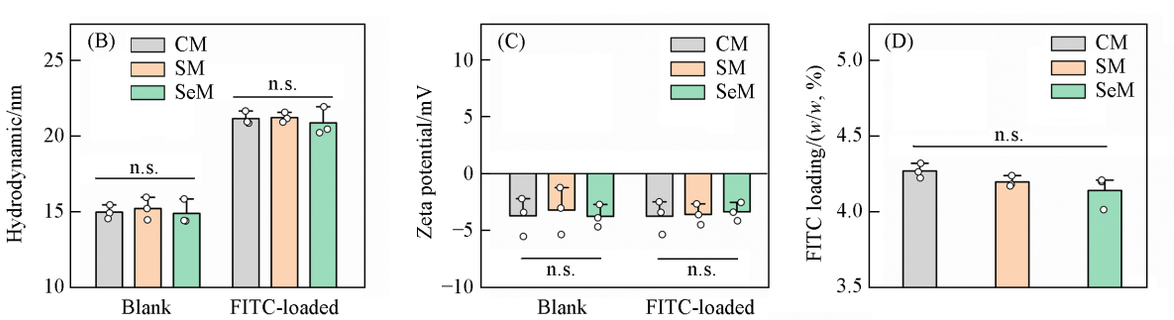


**Fig. 1 Physicochemical assessment of three type of micelles made of *D*-*α*-tocopheryl polyethylene glycol succinate(TPGS) derivatives**

(A) TPGS was conjugated with bifunctional molecule containing a disulfide or diselenide moiety. The disulfide/diselenide-free molecule was used as the control; (B) particle size analysis of three types of micelles with or without the fluorescent cargo (FITC); (C) the surface charge of different types of micelles; (D) the loading of FITC in micelles. Data are presented as mean±standard deviation ($n$=3).

[Fig.1(C)]. The negative surface charge was due to the ionization of carboxyl group ($pK_a$: *ca.* 4.0) at the physiological pH. The loading of FITC in all micelles was maintained the same (*ca.* 4.2%, mass fraction) to aid the intracellular tracking of nanocarrier [Fig.1(D)].

### 3.2 Endocytosis Pathway

Next, we examined the mechanism by which the micelles were internalized at the presence or absence of different endocytosis inhibitors. The human cervical cancer cells(HeLa) were employed as the model and the FITC signal indicted the uptake efficiency. All three types of TPGS conjugate micelles did not show noticeable toxicity up to a dose of 500 μg/mL(Fig.S9, see the Supporting Information of this paper). The endocytosis of nanoparticles is energy-dependent and therefore the cellular uptake of particles was reduced at low temperature. These micelles displayed temperature-dependent cellular uptake, which diminished at 4 ℃ compared to that at 37 ℃[Fig.2(A)—(C)]. Irrespective of micelle type, neither the micropinocytosis inhibitor[5-(*N*-ethyl-*N*-isopropyl)amiloride, EIPA], nor caveolin-mediated endocytosis inhibitor(methyl-beta-cyclodextrin, MβCD) mitigated the intracellular FITC. In contrast, the chlorpromazine(CPZ), a clathrin-mediated endocytosis inhibitor, significantly suppressed the uptake of all three micelles, corrobora-ting the clathrin-mediated nanocarrier internalization[Fig.2(A)—(C)][23]. To examine the thiol-mediated micelle uptake, we employed two thiol-disulfide exchange inhibitors, iodoacetate and 5,5′-dithio-bis-(2-nitrobenzoicacid)(DTNB), to block the thiols at cell surface. Iodoacetate is a haloacetyl that can diminish thiols *via* the thiol-halogen ligation[24]. DTNB depletes the thiols *via* the thiol-disulfide exchange reaction[25]. The presence of either DTNB or iodoacetate did not change the uptake of FITC-CM. However, the internalization of FITC-SM and FITC-SeM was markedly suppressed in the DTNB/iodoacetate-pretreated cells, indicating the thiol-aided cellular uptake of SM and SeM micelles[Fig.2(D)—(F)]. All the selected endocytosis inhibitors and thiol blockers are not toxic at the applied dose(Fig.S10, see the Supporting Information of this paper).

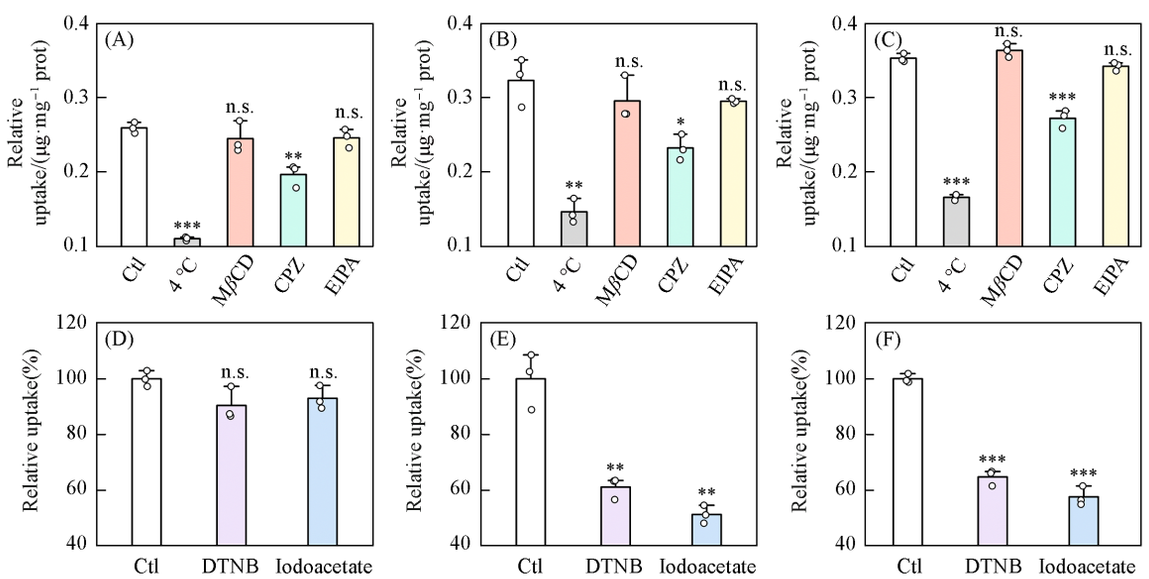


**Fig. 2 Endocytosis pathway of three type of micelles in HeLa cells**

The effect of temperature and endocytosis inhibitors on the uptake of fluorescently labelled micelles: (A) FITC-CM; (B) FITC-SM; (C) FITC-SeM. The influence of thiol blockers on the uptake of micelles: (D) FITC-CM; (E) FITC-SM; (F) FITC-SeM. MβCD, methyl-beta-cyclodextrin; CPZ, chlorpromazine; EIPA, 5-(*N*-ethyl-*N*-isopropyl)amiloride; DTNB, 5,5′-dithio-bis-(2-nitrobenzoic-acid). n.s. indicates no significant difference, * $p$<0.05, ** $p$<0.01, *** $p$<0.001($n$=3).

### 3.3 Cellular Uptake

To test the feasibility of mechanical force-enhanced cellular uptake of nanocarrier, we monitored the micelles uptake at the presence of ultrasound under the previously reported condition(1 MHz, 1.0 W/cm$^2$, 20% duty cycle, 120 s)[26]. Among all three micelles, the extent of uptake by HeLa cells ranked as follows: SeM>SM>CM(Fig.3). The enhanced uptake of SM and SeM in contrast to CM was a consequence of the

exchange reaction between exofacial thiols and the disulfide/diselenide at the micellar surface. However, the kinetics of thiol-diselenide was faster than that of thiol-disulfide, resulting in the facilitated internalization of SeM with reference to SM[27]. The mechanical force did not affect the internalization of CM ($p$>0.05), but the uptake of SM was significantly boosted post ultrasound treatment ($p$<0.001). The uptake of SM was enhanced with increasing ultrasound treatment [Fig.S11(A), see the Supporting Information of this paper]. Likewise, the internalization of SeM was also augmented at the presence of ultrasound ($p$<0.05). The ultrasound was presumed able to enhance the kinetics of thiol-disulfide/diselenide *via* breaking down the transition state complexes. It should be noted that the ultrasound-aided uptake enhancement was more significant for SM other than SeM, which was presumed because of the differences in thiol-disulfide/diselenide reaction kinetics[20,28].

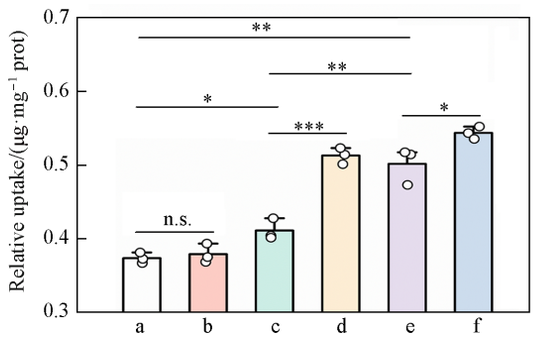


**Fig. 3 Quantification of ultrasound-aided uptake of micelles surface-engineered with disulfide/diselenide in HeLa cells**

a. FITC-CM; b. FITC-CM+US; c. FITC-SM; d. FITC-SM+US; e. FITC-SeM; f. FITC-SeM+US. The effect of ultrasound (US) on the cellular uptake of three types of micelles. US condition: 1 MHz, 1.0 W/cm$^2$, 20% duty cycle, 120 s. n.s. indicates no significant difference, * $p$<0.05, ** $p$<0.01, *** $p$<0.001($n$=3).

### 3.4 Endosomal Escape

To assess the endosomal escape of different types of micelles, we employed two fluorescent probes, FITC and Lysotracker® to track the location of micelles and endosomes/lysosomes (Fig.4). FITC and Lysotracker® display the green and red color, respectively; their overlap produces yellow color, indicating the colocalization. We employed the Pearson's correlation coefficient to examine the colocalization of micelles and

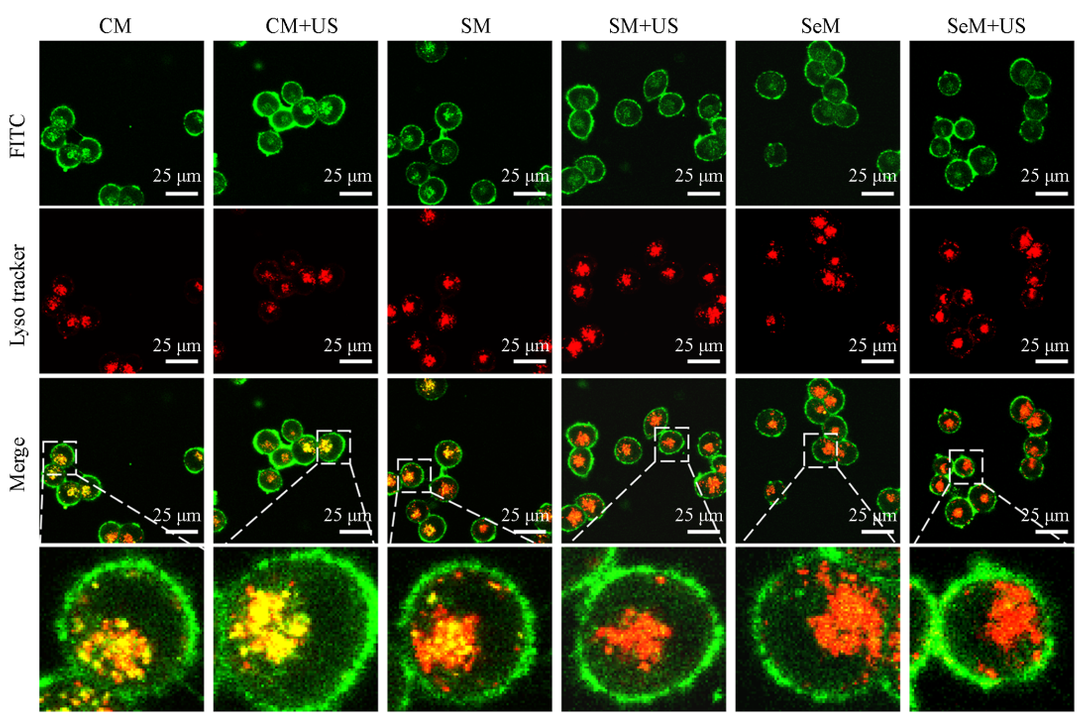


**Fig. 4 Assessment of endosomal escape of three type of micelles in HeLa cells at the presence or absence of ultrasound(US)($n$=3)**

Confocal microscopy images showing the extent of co-localization of FITC-loaded micelles and endosomes/lysosomes. US condition: 1 MHz, 1.0 W/cm$^2$, 20% duty cycle, 120 s.

endosomes/lysosomes. The coefficient value ranges from −1 to +1, indicating a fully negative and positive correlation, respectively[29,30]. At the absence of ultrasound, the Pearson's correlation coefficient ranked as follows: CM>SM>SeM (Fig. 5), suggesting the poorest ability of control micelles in terms of endosomal escape. Both SM and SeM showed the potency of endosomal escape to a certain degree; however, because of the faster thiol-diselenide exchange reaction compared to that of thiol-disulfide counterpart, SeM behaved the best regarding the escape from endosomes/lysosomes.

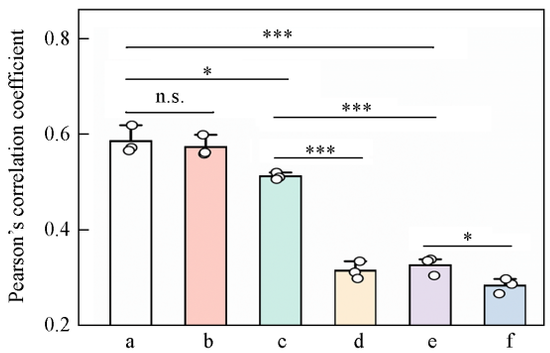


**Fig. 5 Pearson's correlation coefficients reflect endosomal escape capacity of three type of micelles in HeLa cells at the presence or absence of ultrasound(US)**

a. FITC-CM; b. FITC-CM+US; c. FITC-SM; d. FITC-SM+US; e. FITC-SeM; f. FITC-SeM+US. Plot of Pearson's correlation coefficient between FITC-labelled micelles and endosomes/lysosomes indicated by the Lyso Tracker. US condition: 1 MHz, 1.0 W/cm$^2$, 20% duty cycle, 120 s. n. s. indicates no significant difference, * $p$<0.05, ** $p$<0.01, *** $p$<0.001 ($n$=3).

We then investigated into the potency of ultrasound to modulate micelles escape from endosomes/lysosomes. As expected, the mechanical force did not affect the Pearson's correlation coefficient of CM ($p$>0.05), indicating no escape of CM from acidic organelles. In contrast, the Pearson's correlation coefficient of SM ($p$<0.001) and SeM ($p$<0.05) post- and pre-ultrasound corroborated the discharge of micelles out of the endosomes/lysosomes. It seemed that the mechanical force was more potent in facilitating the transport of SM other than SeM out of endosomes/lysosomes, which was presumed because of the different kinetics of thiol-disulfide/diselenide exchange reactions. Moreover, a longer ultrasonic treament resulted in a more significant escape of SM from endosomes/lysosomes [Fig.S11(B)—(C), see the Supporting Information of this paper]. It should be noted that there was a significant accumulation of FITC in the cell membranes (Fig.4). Such behavior can be explained by the non-selective chemical labelling of plasma membrane by the isothiocyanate moiety(—C═N═S) of FITC post release from micelles[31].

The disulfide and diselenide moieties can be facilely attached to the surface of different types of nanocarriers by single-step chemical conjugation. From these regards, nanocarrier surface-engineering with disulfide/diselenide is superior to other active targeting approaches that may involves tedious synthesis and purification processes. Nevertheless, the presence of a large number of disulfide and diselenide moieties may alter the intracellular redox homeostasis by depleting intracellular glutathione (GSH) and reduced nicotinamide adenine dinucleotide phosphate (NADPH), resulting in apoptotic and ferroptotic cell death[32,33]. Moreover, selenium is an essential trace element of humans and a critical component of various enzymes and proteins (*e. g.* selenoproteins). The compactness of these groups on nanocarrier surface can also be manipulated to optimize the targeting effect and endosomal escape ability.

## 4 Conclusions

In summary, the current work highlights the role of mechanical force in enhancing the thiol-disulfide/diselenide exchange reaction that can facilitate cellular uptake and endosomal escape of nanocarriers. Ultrasound has been widely employed in the clinical settings as a non-invasive approach featured with deep tissue penetration. The duration and power of ultrasound can be easily manipulated to modulate the exchange reactions in a spatiotemporal and tailored manner. The nanocarrier surface engineering with disulfide/diselenide could be facilely achieved, which is robust and apply to different types of vehicles,

e. g. liposomes, micelles, and inorganic particles.

The Supporting Information of this paper see http://www.cjcu.jlu.edu.cn/CN/10.7503/cjcu202040265.

## References

[1] Paull R., Wolfe J., Hébert P., Sinkula M., *Nat. Biotechnol.*, **2003**, *21*(10), 1144—1147
[2] Blanco E., Shen H., Ferrari M., *Nat. Biotechnol.*, **2015**, *33*(9), 941—951
[3] Rennick J. J., Johnston A. P. R., Parton R. G., *Nat. Nanotechnol.*, **2021**, *16*(3), 266—276
[4] Pei D. H., Buyanova M., *Bioconjug. Chem.*, **2019**, *30*(2), 273—283
[5] Torres A. G., Gait M. J., *Trends Biotechnol.*, **2012**, *30*(4), 185—190
[6] Digilio G., Menchise V., Gianolio E., Catanzaro V., Carrera C., Napolitano R., Fedeli F., Aime S., *J. Med. Chem.*, **2010**, *53*(13), 4877—4890
[7] Li T., Gao W., Liang J. J., Zha M. R., Chen Y. Q., Zhao Y. B., Wu C. L., *Anal. Chem.*, **2017**, *89*(16), 8501—8508
[8] Shu Z. M., Tanaka I., Ota A., Fushihara D., Abe N., Kawaguchi S., Nakamoto K., Tomoike F., Tada S., Ito Y., Kimura Y., Abe H., *Angew. Chem. Int. Ed.*, **2019**, *58*(20), 6611—6615
[9] Goerdeler F., Reuber E. E., Lühle J., Leichnitz S., Freitag A., Nedielkov R., Groza R., Ewers H., Möller H. M., Seeberger P. H., Moscovitz O., *ACS Cent. Sci.*, **2023**, *9*(6), 1111—1118
[10] Qian L. H., Fu J. Q., Yuan P. Y., Du S. B., Huang W., Li L., Yao S. Q., *Angew. Chem. Int. Ed.*, **2018**, *57*(6), 1532—1536
[11] Chuard N., Gasparini G., Moreau D., Lörcher S., Palivan C., Meier W., Sakai N., Matile S., *Angew. Chem. Int. Ed.*, **2017**, *56*(11), 2947—2950
[12] Zong L. L., Bartolami E., Abegg D., Adibekian A., Sakai N., Matile S., *ACS Cent. Sci.*, **2017**, *3*(5), 449—453
[13] Gasparini G., Sargsyan G., Bang E. K., Sakai N., Matile S., *Angew. Chem. Int. Ed.*, **2015**, *54*(25), 7328—7331
[14] Brea R. J., Devaraj N. K., *ACS Cent. Sci.*, **2017**, *3*(6), 524—525
[15] Kanjilal P., Dutta K., Thayumanavan S., *Angew. Chem. Int. Ed.*, **2022**, *61*(37), e202209227
[16] Li Y. R., Feng S. M., Dai P. P., Liu F., Shang Y. Q., Yang Q., Qin J., Yuchi Z. G., Wang Z., Zhao Y. J., *J. Control. Release*, **2022**, *342*, 201—209
[17] Nagy P., *Antioxid. Redox Signal.*, **2013**, *18*(13), 1623—1641
[18] Fava A., Iliceto A., Camera E., *J. Am. Chem. Soc.*, **1957**, *79*(4), 833—838
[19] Bartolami E., Basagiannis D., Zong L., Martinent R., Okamoto Y., Laurent Q., Ward T. R., Gonzalez-Gaitan M., Sakai N., Matile S., *Chemistry*, **2019**, *25*(16), 4047—4051
[20] Chuard N., Poblador-Bahamonde A. I., Zong L., Bartolami E., Hildebrandt J., Weigand W., Sakai N., Matile S., *Chem. Sci.*, **2018**, *9*(7), 1860—1866
[21] Jensen K. S., Hansen R. E., Winther J. R., *Antioxid. Redox Signal.*, **2009**, *11*(5), 1047—1058
[22] Zhang R. H., Nie T. Q., Fang Y. F., Huang H., Wu J., *Biomacromolecules*, **2022**, *23*(1), 1—19
[23] Song Q., Wang X., Wang Y. Q., Liang Y. Q., Zhou Y. X., Song X. N., He B., Zhang H., Dai W. B., Wang X. Q., Zhang Q., *Mol. Pharm.*, **2016**, *13*(1), 190—201
[24] Tang W., Becker M. L., *Chem. Soc. Rev.*, **2014**, *43*(20), 7013—7039
[25] Simpson R. J., *CSH Protoc.*, **2008**, *2008*, pdb.prot4699
[26] Li Y., Qin Y., Shang Y. Q., Li Y. R., Liu F., Luo J. J., Zhu J. D., Guo X. L., Wang Z., Zhao Y. J., *Adv. Funct. Mater.*, **2022**, *32*(29), 2112000
[27] Canal-Martín A., Pérez-Fernández R., *Nat. Commun.*, **2021**, *12*(1), 163
[28] Laurent Q., Martinent R., Lim B., Pham A. T., Kato T., López-Andarias J., Sakai N., Matile S., *JACS Au*, **2021**, *1*(6), 710—728
[29] French A. P., Mills S., Swarup R., Bennett M. J., Pridmore T. P., *Nat. Protoc.*, **2008**, *3*(4), 619—628
[30] Chen C., Tao R., Ding D., Kong D. L., Fan A. P., Wang Z., Zhao Y. J., *Eur. J. Pharm. Sci.*, **2017**, *107*, 16—23
[31] Chaganti L. K., Venkatakrishnan N., Bose K., *Biosci. Rep.*, **2018**, *38*(6), BSR20181764
[32] Meng X., Deng J., Liu F., Guo T., Liu M. Y., Dai P. P., Fan A. P., Wang Z., Zhao Y. J., *Nano Lett.*, **2019**, *19*(11), 7866—7876
[33] Guo X. L., Liu F., Deng J., Dai P. P., Qin Y., Li Z., Wang B. B., Fan A. P., Wang Z., Zhao Y. J., *ACS Nano*, **2020**, *14*(11), 14715—14730

(Ed.: L, W, K)